

Engineering two-dimensional nodal semimetals in functionalized biphenylene by fluorine adatoms

Seongjun Mo,^{1,*} Jaeuk Seo,^{2,3,*} Seok-Kyun Son,^{4,5} Sejoong Kim,^{6,7,†} Jun-Won Rhim,^{2,8,‡} and Hoonkyung Lee^{1,8,§}

¹*Department of Physics, Konkuk University, Seoul 05029, Korea*

²*Department of Physics, Ajou University, Suwon 16499, Korea*

³*Department of Physics, Korea Advanced Institute of Science and Technology, Daejeon 34141, Korea*

⁴*Department of Physics, Kyung Hee University, Seoul 02447, Republic of Korea*

⁵*Department of Information Display, Kyung Hee University, Seoul 02447, Republic of Korea*

⁶*University of Science and Technology (UST), Gajeong-ro 217, Daejeon 34113, Korea*

⁷*Korea Institute for Advanced Study, Hoegiro 85, Seoul 02455, Korea*

⁸*Research Center for Novel Epitaxial Quantum Architectures,
Department of Physics, Seoul National University, Seoul, 08826, Korea*

We propose a new band engineering scheme on the biphenylene network, a newly synthesized carbon allotrope. First, we investigate the mechanism for the appearance of type II Dirac fermion in a pristine biphenylene network. We show that the essential ingredients are mirror symmetries and the stabilization of the compact localized eigenstates via destructive interference. While the former is used for the band-crossing point along high symmetry lines, the latter makes the obtained Dirac dispersion highly inclined. Then, we demonstrate that many other different kinds of Dirac fermions, such as type-I Dirac, gapped type-II Dirac, and nodal line semimetals, can be developed by fluorinating the biphenylene network periodically in various ways. In this program, the key role of the fluorine atoms is manipulating the condition of the destructive interference and mirror symmetries.

I. INTRODUCTION

Triggered by the discovery of carbon nanotubes^{1,2}, studies on low dimensional carbon allotropes, such as graphene, have significantly proliferated because one can have a variety of intriguing electronic structures depending on the arrangement of carbon atoms. For example, one can have massless Dirac fermions in graphene^{3,4}, whereas infinitely heavy particles can also ap-

pear in another honeycomb network of carbon atoms called the cyclic-graphdiyne, which hosts a singular flat band^{5,6}. In the case of graphene, relying on its high structural stability, one can further engineer the band structure to obtain flat bands by tailoring it into ribbon geometries⁷ or twisting two stacked graphene sheets^{8,9}. These peculiar electronic structures have received great attention because they are relevant to the possible many-body phases such as ferromagnetism^{10,11} and superconductivity¹²⁻¹⁵.

Recently, another type of two-dimensional carbon allotrope, called the biphenylene network (BPN), was synthesized¹⁶ and has attracted significant interests in various properties of BPN layers including electronic, optical, mechanical, thermal, magnetic and chemical properties¹⁷⁻⁵³. Moreover, from the first principles analysis, BPN turned out to exhibit another intriguing band dispersion called type-II Dirac fermion consisting of two heavily inclined cones, so that we have open Fermi surfaces instead of Fermi points or circles^{17,18}. In type-II Dirac semimetals⁵⁴, one can have electron- and hole-type carriers simultaneously in contrast to the type-I case such as graphene. This intricate band shape may lead to a variety of unusual electronic phenomena such as anisotropic transport and magnetoresistance behavior⁵⁵⁻⁵⁸ and undamped gapless plasmon modes⁵⁹. Therefore, engineering their band shapes is important to tune the electronic properties for applications.

In this paper, we first analyze the origin of the type-II Dirac dispersion of the pristine BPN from the perspective of destructive interference and symmetry. The essential feature of the type-II Dirac dispersion of the pristine BPN is that it is inclined so that a flat band with a zero Fermi velocity appears along a high symmetry line while the Dirac band-crossing is protected by mirror symmetry. We show that the the pristine BPN hosts a proper destructive interference stabilizing a stripe-type compact localized state, which signals the existence of a flat band, along the mirror-symmetric axis in momentum space. This implies that one can engineer the electronic structures of the BPN by controlling the condition for destructive interference and symmetries. We demonstrate that this can be done successfully by absorbing fluorine atoms at various positions. We show that we can have diverse Dirac dispersions of different kinds, such as type-I, massive, and nodal line Dirac fermions, by fluorinating BPN periodically.

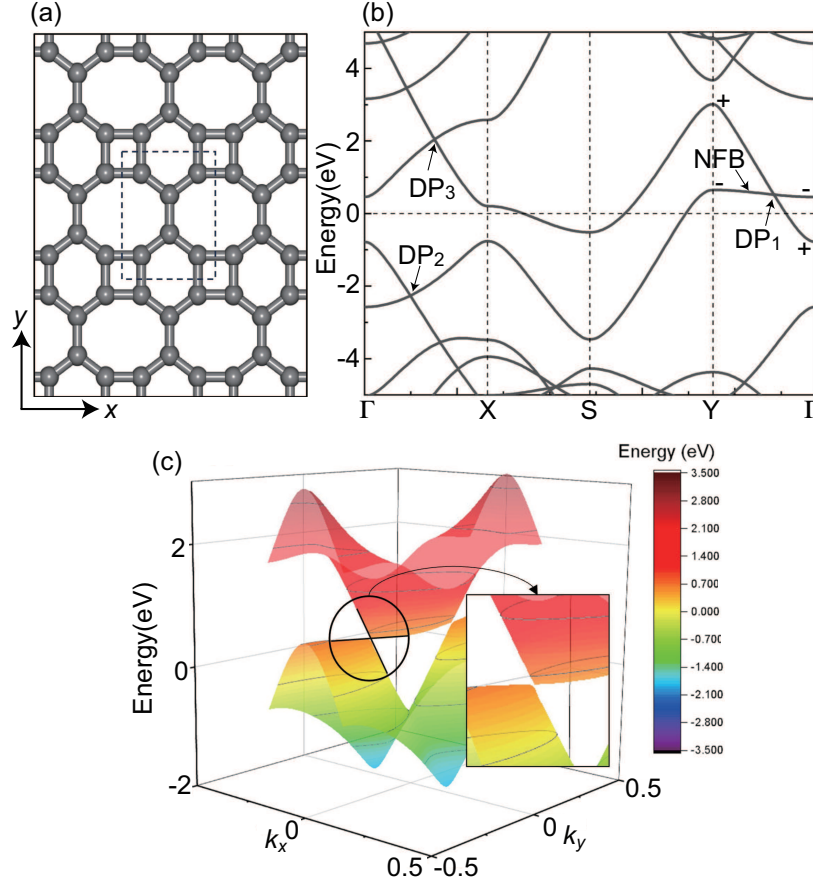


FIG. 1: (a) The lattice structure, (b) band structure, and (c) 3D energy structure near the ΓY line of pristine BPN. The unit cell is represented by a dashed box in (a). Several Dirac points are denoted by DP_1 , DP_2 , and DP_3 , in (b). NFB indicates the nearly flat band.

II. RESULTS AND DISCUSSION

A. First-principles calculations

To investigate the geometrical and electronic properties of pristine single-layer BPN, we perform geometry optimization of BPN using first-principles calculations based on density functional theory (DFT). The optimized geometry and energy bands of BPN are shown in Fig. 1(a) and (b), respectively. As in the previous study^{17,18}, we observe a couple of type-II Dirac points whose Dirac nodes lie on ΓY near the Fermi energy E_F as denoted by DP_1 in Fig. 1(b). As highlighted in Fig. 1(c), there are two tilted Dirac dispersions around the Γ point. corresponding to DP_1 in Fig. 1(b). While the Dirac point is developed by the crossing of two bands along ΓY , it is essential that one of them is almost flat for realizing a type-II Dirac fermion. Therefore, it is crucial to

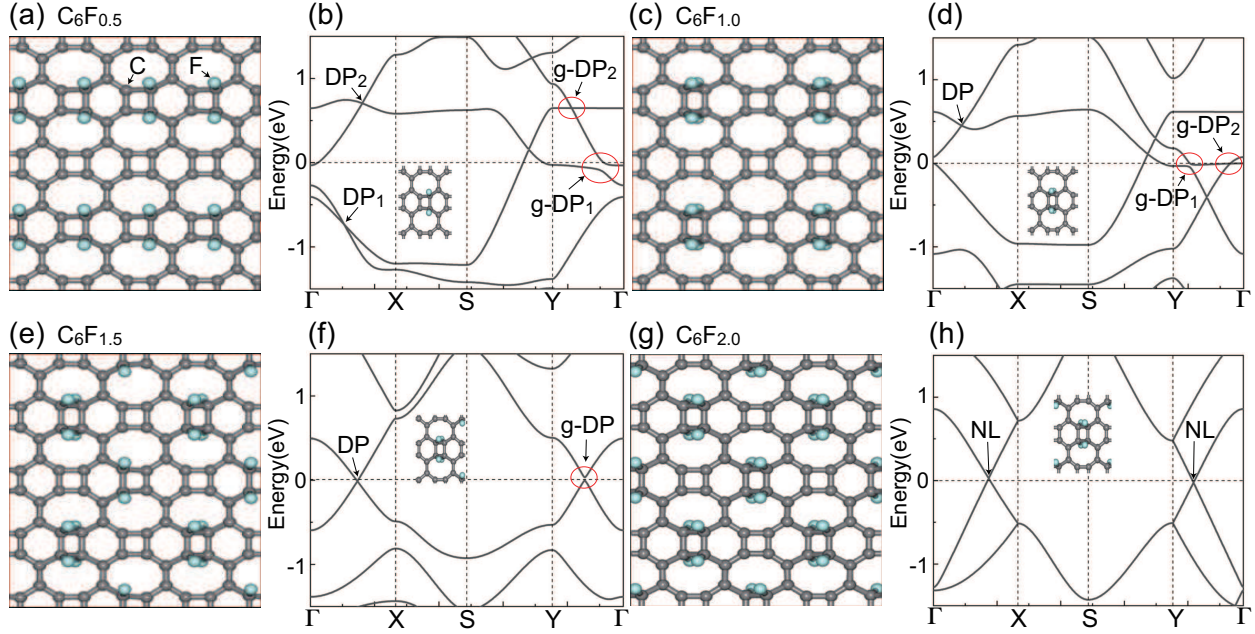


FIG. 2: Optimized geometries of fluorinated BPN monolayers with different concentrations of fluorine and their electronic structures: (a,b) $C_6F_{0.5}$, (c,d) $C_6F_{1.0}$, (e,f) $C_6F_{1.5}$, and (g,h) $C_6F_{2.0}$. Gray (Cyan) spheres represent carbon (fluorine) atoms. Dirac nodes, gapped-Dirac points, and nodal lines are denoted by DP, g-DP, and NL, respectively.

understand the origin of the flat dispersion along ΓY to reveal the mechanism for the appearance of the type-II Dirac semimetal, and it will be discussed in the following subsection.

We introduce fluorine atoms to a single-layer BPN to engineer its electronic structures. Regarding a pristine BPN monolayer, binding energies of fluorine (F) atoms to carbon sites are computed as follows: 3.20 eV/F for square, 2.21 eV/F for hexagon, and 2.10 eV/F for octagon. It implies that F atoms energetically prefer to bind to a square unit rather than hexagon and octagon units. Varying fluorine concentrations x , we consider four fluorinated BPN layers C_6F_x for $x = 0.5, 1.0, 1.5$, and 2.0, whose atomic structures are displayed in Figs. 2(a), (c), (e), and (g), respectively. DFT calculations also reveal that F atoms energetically prefer to attach to square sites for higher F concentrations. Corresponding binding energies of F to square units are 3.45, 3.51, 3.48, and 3.50 eV/F for $x = 0.5, 1.0, 1.5$, and 2.0, respectively. Note that due to sp^3 hybridization the bond between C and F is not perpendicular to single layer BPN.

Band structures of the fluorinated BPNs are plotted on the right side of atomic configurations in Fig. 2. Intriguingly, diverse nodal states emerge depending on F concentrations. At fluorine concentrations of 0.5 and 1.0, gapped type-II Weyl nodes are found as a result of crossing between

flat bands near E_F along ΓY and energy bands hosting saddle-point van Hove singularity (vHS) at Y . See red circles in Figs. 2(b) and (d). These gap opening is attributed to the mirror symmetry breaking with respect to monolayer BPN plane due to fluorine attachment. On the other hand, we found gapless and gapped type-I Dirac points along x - and y -axis in $C_6F_{1.5}$ as shown in Fig. 2(f) while nodal rings appear in C_6F_2 as noted in Fig. 2(h). For clarity, we provide 3D band structures of these two compounds in Supplementary Fig. 3. An effective Hamiltonian is formulated using a tight-binding model in the next subsection to provide a more accurate interpretation.

To understand how the variety of relativistic dispersions can be stabilized in pristine BPN and fluorinated BPNs, we conduct an analysis of their wave function symmetries. Here, we first focus on protection or gap-opening mechanisms of the nodal points or lines, while the origin of the inclination in Dirac dispersions is addressed in the next subsection. Specifically, we only consider the wave functions of the bands near the Fermi level. The symmetries of the wave functions are visualized by plotting the amplitudes of the Bloch wave function at Γ point as illustrated in Supplementary Fig. 1. For the pristine BPN, one can show that the band-crossing along ΓY in Fig. 1(b) is protected by the mirror symmetry with respect to yz plane, which is denoted by M_x . The nearly flat band (NFB) and the dispersive band, which constitute the type-II Dirac point, correspond to the mirror eigenvalue -1 and 1, respectively, as shown in Supplementary Fig. 1(a). Furthermore, upon close inspection of the wave function depicted in Supplementary Figure 1(a), an intriguing resemblance to the anti-bond wave function of benzene becomes apparent. This finding may imply a potential connection between the electronic properties of the material under investigation and those of benzene, which is known for its aromatic properties and unique bonding characteristics.

On the other hand, the mirror symmetry M_x is broken in $C_6F_{0.5}$ and C_6F_1 . As a result, the wave functions are not mirror-symmetric with respect to yz plane as shown in Supplementary Figure 1(b) and (c), and band crossings along ΓY are all gapped out, realizing massive type-II Dirac fermions as shown in Figs. 2(b) and (d). Although several type-II Dirac nodes, denoted by g-DP₂ in Fig. 2(b) and (d), looks gapless, they actually have tiny gaps. Note that $C_6F_{0.5}$ and C_6F_1 respect the mirror symmetry M_y with respect to zx plane, so their wave functions are either mirror symmetric or mirror anti-symmetric as illustrated in as illustrated in Supplementary Figure 1(b) and (c). Thus band-crossings indicated by DP₁ and DP₂ in Fig. 2(b) and DP in Fig. 2(d), are protected along ΓX . As like the two previous compounds, $C_6F_{1.5}$ satisfies only the mirror symmetry M_y , so it has gapless and gapped-out Dirac nodes on ΓX and ΓY , respectively. See

Fig. 2(f). In contrast to $C_6F_{0.5}$ and C_6F_1 , $C_6F_{1.5}$ does not stabilize flat bands, resulting exclusively in type-I Dirac fermions. Finally, in C_6F_2 , both mirror symmetries M_x and M_y are respected. The system, therefore, becomes gapless along both ΓX and ΓY as illustrated in Fig. 2(h). In fact, these two nodes are part of the nodal line.

B. Tight-binding analysis

In this subsection, we discuss another crucial condition for the appearance of type-II Dirac fermions in pristine BPN and aforementioned fluorinated BPNs by analyzing how flat bands are stabilized along certain symmetry axes. To this end, we apply a tight-binding method, which is advantageous for the flat band analysis. The essential mechanism for the development of the dispersionless band is the existence of a compact localized state (CLS), which is a localized eigenstate having nonzero amplitudes only inside a finite region^{60–63}. Although electrons can move on the lattice via hopping processes, such an extremely localized mode can exist due to the destructive interference hosted by the special lattice structures. The CLS is considered a characteristic eigenstate of a flat band because it is guaranteed to exist when it is completely flat⁶². While one can have N (the number of unit cells) different CLSs centered at different positions, they are not independent of each other if the Bloch eigenstate corresponding to the flat band possesses a discontinuity in momentum space. Such a flat band is called a singular flat band, and its geometric and topological aspects have been studied extensively^{6,62–65}.

First, regarding that energy bands of our interest mostly originate from p_z orbitals of carbon atoms, we construct an effective tight-binding model consisting of the six p_z orbitals for the pristine BPN to understand the origin of its flat bands along ΓY and XS , as shown in Fig. 3(a). Along these lines, the Hamiltonian can be regarded effectively as a one-dimensional system hosting flat bands. The effective 1D Hamiltonian along ΓY and XS are obtained by the inverse Fourier transform of the Bloch Hamiltonian with $k_x = 0$ and $k_x = \pi$, respectively. Therefore, we seek a CLS compactly localized along y -axis in order to understand the origin of flat bands. Six tight-binding parameters are denoted by t_{sx} , t_{sy} , t_y , t_d , t_s , and t_p as represented in Fig. 3(c). Main features of the DFT calculations can be captured by the tight-binding parameters $\{t_{sx}, t_{sy}, t_y, t_d, t_s, t_p, E_0\} = \{-3, -2.7, -2.7, -2.8, -0.7, -0.3, -0.5\}$, where E_0 is the overall energy shift. Two perfectly flat bands around the Fermi level along ΓY and XS are denoted by $F1$ and $F2$, respectively. Their energies are given by $E_{F1} = -t_p - t_s + t_{sx} - t_{sy} + E_0$ and $E_{F2} = -t_p - t_s - t_{sx} + t_{sy} + E_0$.

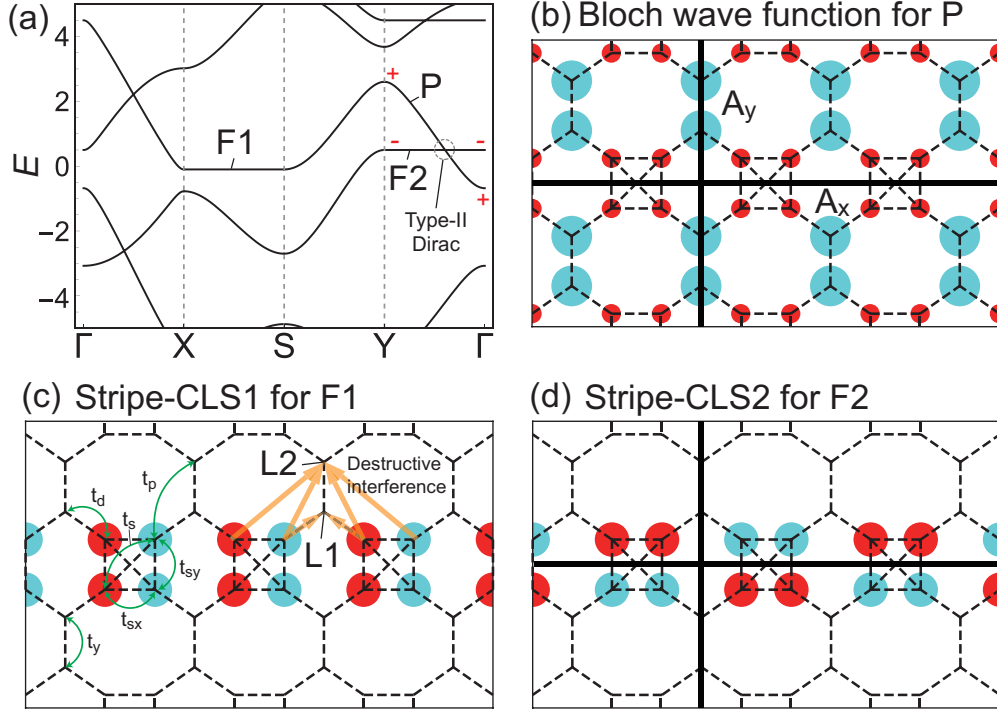


FIG. 3: (a) The tight-binding band structures of the pristine BPN with band parameters $\{t_{sx}, t_{sy}, t_y, t_d, t_s, t_p, E_0\} = \{-3, -2.7, -2.7, -2.8, -0.7, 0, -0.5\}$. We indicate the 1D flat bands along XS and Y Γ by F1 and F2, respectively. The parabolic band crossing with the flat band F2 is denoted by P. (b) The Bloch wave function corresponding to the parabolic band P at Γ . Colored circles represent the amplitudes of the wave function. Red (cyan) color implies that the sign of the amplitude is 1 (-1), while the radius of the circle is proportional to the magnitude of the amplitude. Thick vertical and horizontal lines represent the mirror symmetry planes. In (c) and (d), we illustrate the stripe-CLS1 and stripe-CLS2 corresponding to the flat bands F1 and F2, respectively. In (c), the hopping processes are summarized. The CLS can be an eigenmode even if the longer-ranged hopping processes represented by the yellow arrow are further included due to the destructive interference at sites L1 and L2.

The flatness of these flat bands is robust against the variation of those tight-binding parameters. The CLSs corresponding to the flat bands F1 and F2 are plotted in Fig. 3(c) and (d). As the effective Hamiltonians are translationally invariant along y -axis, the CLSs are compactly localized along the same direction. On the other hand, they are extended along x -direction modulating with the fixed momenta $k_x = 0$ and $k_x = \pi$. These CLSs are denoted as the stripe-CLSs. One can notice that the lattice structure provides a destructive interference at the sites linking two neighboring square plaquettes of carbon atoms, denoted by L_1 , as explained in Fig. 3(c). While the

flat band $F2$ has a Dirac band-crossing with a dispersive band, this is protected by mirror symmetry M_x because the CLS and the wave functions in the dispersive band have mirror eigenvalues -1 and $+1$, respectively, as shown in Fig. 3(b) and (d). This band-crossing between the flat and dispersive bands results in type-II Dirac fermion, as plotted in Fig. 3(a). Note that a long-range hopping t_p does not break the flatness of the flat band because this hopping process also offers another destructive interference for the same CLS, denoted by L_2 in Fig. 3(c). Although the longer-ranged hybridizations would not provide such a destructive interference and, therefore, deform the flat band, the resultant bandwidth is tiny, as we observed in DFT calculations, because their hopping amplitudes should be much smaller than the nearest neighbor ones. Even if the flat band is warped, the band-crossing is robust against the inclusion of the long-range processes because mirror symmetry is still respected. The pristine BPN has another mirror symmetry M_y , and the type-I Dirac dispersions along ΓX are protected by it.

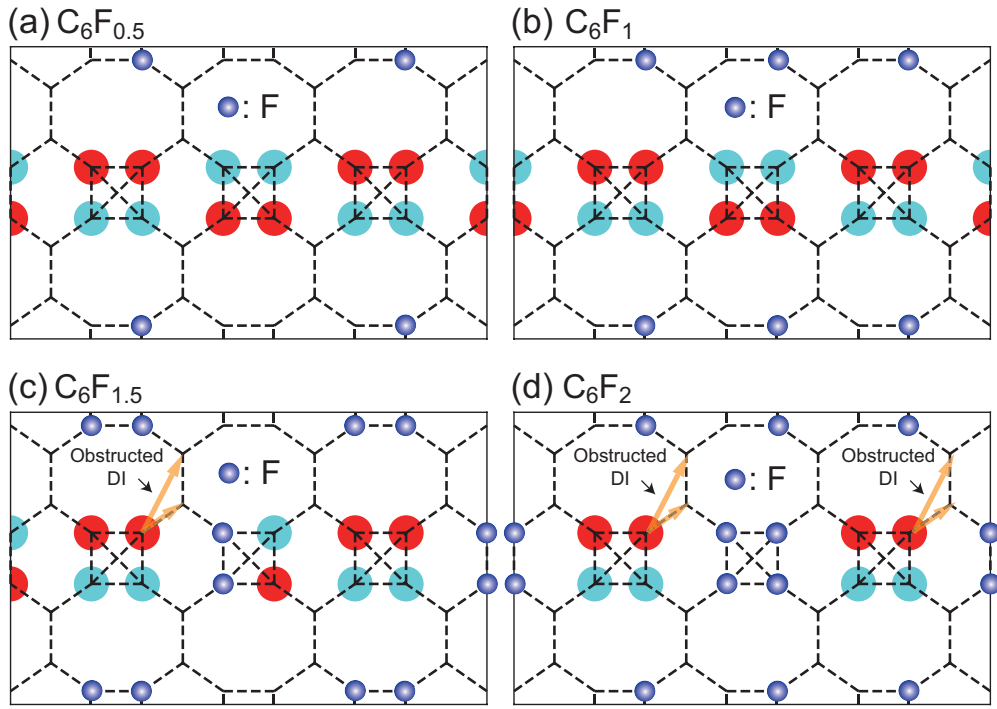


FIG. 4: In (a) and (b), the stripe-CLSs of $C_6F_{0.5}$ and C_6F_1 are plotted. They are occupying the chain of square plaquettes of carbon atoms in the middle. The attached fluorine atoms are represented by blue circles. The red and cyan circles mean plus and minus signs, respectively. In (c) and (d), we show that the stabilization of the stripe-CLSs fails due to the obstructed destructive interference(DI) by fluorine atoms in the middle chain of the square plaquettes.

As a next step, we show that by fluorinating BPN, such as $C_6F_{0.5}$ and C_6F_1 , we can have gapped type-II Weyl semimetals. In the tight-binding analysis, the fluorination is assumed to be equivalent to making a vacancy at the corresponding carbon site. This assumption is reasonable since hybridization between p_z orbital and fluorine atoms leads to bonding and anti-bonding states whose energies might be pushed away from the energy window of our interest. For $C_6F_{0.5}$ and C_6F_1 , stripe-CLSs can still be stabilized along the chain of square plaquettes of carbon atoms, which are not fluorinated and extended along x -axis, as shown in Fig. 4(a) and (b). As a result, the flat bands appear along ΓY and $X S$, as shown by the nearly flat bands in DFT band structures in Fig. 2(b) and (d). However, due to the broken mirror symmetry by the fluorine atoms, any band-crossing along these high-symmetry lines does not have to be protected. Indeed, all the band-crossings of type-II Dirac dispersions along ΓY are gapped out, as discussed in the previous subsection. In the case of $C_6F_{0.5}$, we note that the energy gap at the higher Dirac point (g-DP₂) is tiny but nonzero. Namely, we obtained massive type-II Dirac fermions by fluorination, which breaks mirror symmetry while maintaining destructive interference. Since the attached fluorine atoms do not break M_y , type-I Dirac dispersions along ΓX and $S Y$ are all immune from being gapped out. If we attach more fluorine atoms, any stripe-CLSs cannot be an eigenmode because all the possible destructive interferences are obstructed by the fluorine atoms, as shown in Fig. 4(c) and (d). Therefore, we cannot expect flat bands in $C_6F_{1.5}$ and C_6F_2 , and no type-II Dirac semimetals are expected in these compounds. Instead, type-I and nodal line semimetals appear, as shown in DFT calculations.

III. CONCLUSION

In this paper, we have shown that a variety of Dirac particles, such as massless or massive type-I and -II Dirac, and a nodal line can be obtained by the manipulated fluorination on the BPN. In our band engineering scheme, it is crucial that one can eliminate destructive interferences and mirror symmetries by properly locating the fluorine atoms. While we have focused on a specific material system, our work eventually proposes a novel band engineering method, where we control the slope of a part of Dirac dispersion by manipulating the condition for destructive interference via the molecular absorption technique.

Attaching atoms on two-dimensional lattices or surfaces on a microscopic level is experimentally feasible. By using scanning tunneling microscopy (STM), hydrogen atoms or CO molecules

can be absorbed and controlled on graphene or Cu(111) surface on the atomic scale^{66,67}, and even an automated manipulation of their position is possible⁶⁸. Moreover, the fluorination of another carbon allotrope, graphene, has been extensively studied^{69–73}. Therefore, we believe that our band engineering scheme can be realized in experiments so that fluorinated BPN could be an ideal platform to study intriguing phenomena from various types of Dirac dispersions and flat bands.

Acknowledgments

H.L and J.W.R are supported by the National Research Foundation of Korea (NRF) Grant funded by the Korean government (MSIT) (Grant no. 2021R1A5A1032996). J.W.R is supported by the National Research Foundation of Korea (NRF) Grant funded by the Korean government (MSIT) (Grant no. 2021R1A2C1010572 and 2022M3H3A106307411) and the Ministry of Education(Grant no. RS-2023-00285390). S.K is supported by the National Research Foundation of Korea (NRF) grant funded by the Korea government (Grant No. NRF-2022R1F1A1074670). S.K.S acknowledges the support by the National Research Foundation of Korea(NRF) grant funded by the Korea government(MSIT) (2022R1A5A8033794).

* These authors contributed equally to this work

† Electronic address: sejoong@alum.mit.edu

‡ Electronic address: jwrhim@ajou.ac.kr

§ Electronic address: hklee3@konkuk.ac.kr

¹ S. Iijima, Helical microtubules of graphitic carbon, *Nature* **354**, 56 (1991).

² M. Dresselhaus, G. Dresselhaus, and R. Saito, Physics of carbon nanotubes, *Carbon* **33**, 883 (1995), nanotubes.

³ K. S. Novoselov, A. K. Geim, S. V. Morozov, D.-e. Jiang, Y. Zhang, S. V. Dubonos, I. V. Grigorieva, and A. A. Firsov, Electric field effect in atomically thin carbon films, *science* **306**, 666 (2004).

⁴ Y. Zhang, Y.-W. Tan, H. L. Stormer, and P. Kim, Experimental observation of the quantum hall effect and berry's phase in graphene, *nature* **438**, 201 (2005).

⁵ J.-Y. You, B. Gu, and G. Su, Flat band and hole-induced ferromagnetism in a novel carbon monolayer, *Scientific Reports* **9**, 20116 (2019).

- ⁶ J.-W. Rhim, K. Kim, and B.-J. Yang, Quantum distance and anomalous Landau levels of flat bands, *Nature* **584**, 59 (2020).
- ⁷ Y.-W. Son, M. L. Cohen, and S. G. Louie, Energy gaps in graphene nanoribbons, *Phys. Rev. Lett.* **97**, 216803 (2006).
- ⁸ Y. Cao, V. Fatemi, S. Fang, K. Watanabe, T. Taniguchi, E. Kaxiras, and P. Jarillo-Herrero, Unconventional superconductivity in magic-angle graphene superlattices, *Nature* **556**, 43 (2018).
- ⁹ G. Tarnopolsky, A. J. Kruchkov, and A. Vishwanath, Origin of magic angles in twisted bilayer graphene, *Phys. Rev. Lett.* **122**, 106405 (2019).
- ¹⁰ A. Mielke, Ferromagnetism in the Hubbard model and Hund's rule, *Physics Letters A* **174**, 443 (1993).
- ¹¹ H. Tasaki, From Nagaoka's ferromagnetism to flat-band ferromagnetism and beyond: an introduction to ferromagnetism in the Hubbard model, *Progress of Theoretical Physics* **99**, 489 (1998).
- ¹² G. Volovik, The Fermi condensate near the saddle point and in the vortex core, *JETP Letters* **59**, 830 (1994).
- ¹³ L. Balents, C. R. Dean, D. K. Efetov, and A. F. Young, Superconductivity and strong correlations in moiré flat bands, *Nature Physics* **16**, 725 (2020).
- ¹⁴ V. Peri, Z.-D. Song, B. A. Bernevig, and S. D. Huber, Fragile topology and flat-band superconductivity in the strong-coupling regime, *Physical Review Letters* **126**, 027002 (2021).
- ¹⁵ G. E. Volovik, Graphite, graphene, and the flat band superconductivity, *JETP Letters* **107**, 516 (2018).
- ¹⁶ Q. Fan, L. Yan, M. W. Tripp, O. Krejčí, S. Dimosthenous, S. R. Kachel, M. Chen, A. S. Foster, U. Koert, P. Liljeroth, and J. M. Gottfried, Biphenylene network: A nonbenzenoid carbon allotrope, *Science* **372**, 852 (2021).
- ¹⁷ Y.-W. Son, H. Jin, and S. Kim, Magnetic ordering, anomalous Lifshitz transition, and topological grain boundaries in two-dimensional biphenylene network, *Nano Letters* **22**, 3112 (2022).
- ¹⁸ P.-F. Liu, J. Li, C. Zhang, X.-H. Tu, J. Zhang, P. Zhang, B.-T. Wang, and D. J. Singh, Type-II Dirac cones and electron-phonon interaction in monolayer biphenylene from first-principles calculations, *Phys. Rev. B* **104**, 235422 (2021).
- ¹⁹ S. Demirci, i. m. c. Çallıoğlu, T. Görkan, E. Aktürk, and S. Ciraci, Stability and electronic properties of monolayer and multilayer structures of group-IV elements and compounds of complementary groups in biphenylene network, *Phys. Rev. B* **105**, 035408 (2022).
- ²⁰ Y. Luo, C. Ren, Y. Xu, J. Yu, S. Wang, and M. Sun, A first principles investigation on the structural, mechanical, electronic, and catalytic properties of biphenylene, *Scientific Reports* **11**, 19008 (2021).

- ²¹ P. Rublev, N. V. Tkachenko, and A. I. Boldyrev, Overlapping electron density and the global delocalization of π -aromatic fragments as the reason of conductivity of the biphenylene network, *Journal of Computational Chemistry* **44**, 168 (2023).
- ²² G. Liu, T. Chen, X. Li, Z. Xu, and X. Xiao, Electronic transport in biphenylene network monolayer: Proposals for 2D multifunctional carbon-based nanodevices, *Applied Surface Science* **599**, 153993 (2022).
- ²³ S. Chowdhury, S. Ghosal, D. Mondal, and D. Jana, First-principles and machine-learning study of electronic and phonon transport in carbon-based AA-stacked bilayer biphenylene nanosheets, *Journal of Physics and Chemistry of Solids* **170**, 110909 (2022).
- ²⁴ H. Shen, R. Yang, K. Xie, Z. Yu, Y. Zheng, R. Zhang, L. Chen, B.-R. Wu, W.-S. Su, and S. Wang, Electronic and optical properties of hydrogen-terminated biphenylene nanoribbons: a first-principles study, *Phys. Chem. Chem. Phys.* **24**, 357 (2022).
- ²⁵ Y. Xie, L. Chen, J. Xu, and W. Liu, Effective regulation of the electronic properties of a biphenylene network by hydrogenation and halogenation, *RSC Adv.* **12**, 20088 (2022).
- ²⁶ K. Wang, K. Ren, D. Zhang, Y. Cheng, and G. Zhang, Phonon properties of biphenylene monolayer by first-principles calculations, *Applied Physics Letters* **121**, 042203 (2022).
- ²⁷ A. Hamed Mashhadzadeh, M. Zarghami Dehaghani, F. Molaie, S. Fooladapanjeh, O. Farzadian, and C. Spitas, A theoretical insight into the mechanical properties and phonon thermal conductivity of biphenylene network structure, *Computational Materials Science* **214**, 111761 (2022).
- ²⁸ B. Mortazavi and A. V. Shapeev, Anisotropic mechanical response, high negative thermal expansion, and outstanding dynamical stability of biphenylene monolayer revealed by machine-learning interatomic potentials, *FlatChem* **32**, 100347 (2022).
- ²⁹ M. L. Pereira, W. F. da Cunha, R. T. de Sousa, G. D. Amvame Nze, D. S. Galvão, and L. A. Ribeiro, On the mechanical properties and fracture patterns of the nonbenzenoid carbon allotrope (biphenylene network): a reactive molecular dynamics study, *Nanoscale* **14**, 3200 (2022).
- ³⁰ X. Ren, K. Wang, Y. Yu, D. Zhang, G. Zhang, and Y. Cheng, Tuning the mechanical anisotropy of biphenylene by boron and nitrogen doping, *Computational Materials Science* **222**, 112119 (2023).
- ³¹ A. Bafekry, M. Faraji, M. M. Fadlallah, H. R. Jappor, S. Karbasizadeh, M. Ghergherehchi, and D. Gogova, Biphenylene monolayer as a two-dimensional nonbenzenoid carbon allotrope: a first-principles study, *Journal of Physics: Condensed Matter* **34**, 015001 (2021).
- ³² N. Yang, Q. Chen, Y. Xu, J. Luo, H. Yang, and G. Jin, Strain-modulated electronic transport in two-dimensional carbon allotropes, *AIP Advances* **12**, 045102 (2022).

- ³³ L. Zhang and P. Tong, Even-odd chain dependent spin valve effect on a zigzag biphenylene nanoribbon junction, *Journal of Physics: Condensed Matter* **34**, 395301 (2022).
- ³⁴ I. Alcón, G. Calogero, N. Papior, A. Antidormi, K. Song, A. W. Cummings, M. Brandbyge, and S. Roche, Unveiling the multiradical character of the biphenylene network and its anisotropic charge transport, *Journal of the American Chemical Society* **144**, 8278 (2022), pMID: 35476458.
- ³⁵ K. Ren, H. Shu, W. Huo, Z. Cui, and Y. Xu, Tuning electronic, magnetic and catalytic behaviors of biphenylene network by atomic doping, *Nanotechnology* **33**, 345701 (2022).
- ³⁶ Y. Ge, Z. Wang, X. Wang, W. Wan, and Y. Liu, Superconductivity in the two-dimensional nonbenzenoid biphenylene sheet with Dirac cone, *2D Materials* **9**, 015035 (2021).
- ³⁷ G.-H. Liu, L. Yang, S.-X. Qiao, N. Jiao, Y.-J. Chen, M.-Y. Ni, M.-M. Zheng, H.-Y. Lu, and P. Zhang, Superconductivity of monolayer functionalized biphenylene with Dirac cones, *Phys. Chem. Chem. Phys.* **25**, 2875 (2023).
- ³⁸ H. P. Veeravenkata and A. Jain, Density functional theory driven phononic thermal conductivity prediction of biphenylene: A comparison with graphene, *Carbon* **183**, 893 (2021).
- ³⁹ P. Zhang, T. Ouyang, C. Tang, C. He, J. Li, C. Zhang, M. Hu, and J. Zhong, The intrinsic thermal transport properties of the biphenylene network and the influence of hydrogenation: a first-principles study, *J. Mater. Chem. C* **9**, 16945 (2021).
- ⁴⁰ Z. Tong, A. Pecchia, C. Yam, T. Dumitrică, and T. Frauenheim, Ultrahigh electron thermal conductivity in T-graphene, biphenylene, and net-graphene, *Advanced Energy Materials* **12**, 2200657 (2022).
- ⁴¹ Q. Li, J. Zhou, G. Liu, and X. Wan, Extraordinary negative thermal expansion of monolayer biphenylene, *Carbon* **187**, 349 (2022).
- ⁴² Z.-X. Xie, X.-K. Chen, X. Yu, Y.-X. Deng, Y. Zhang, W.-X. Zhou, and P.-Z. Jia, Intrinsic thermoelectric properties in biphenylene nanoribbons and effect of lattice defects, *Computational Materials Science* **220**, 112041 (2023).
- ⁴³ G. Yang, Y. Hu, Z. Qiu, B.-L. Li, P. Zhou, D. Li, and G. Zhang, Abnormal strain-dependent thermal conductivity in biphenylene monolayer using machine learning interatomic potential, *Applied Physics Letters* **122**, 082202 (2023).
- ⁴⁴ T. Liu, Y. Jing, and Y. Li, Two-dimensional biphenylene: A graphene allotrope with superior activity toward electrochemical oxygen reduction reaction, *The Journal of Physical Chemistry Letters* **12**, 12230 (2021), pMID: 34928622.
- ⁴⁵ P. Mane, S. P. Kaur, and B. Chakraborty, Enhanced reversible hydrogen storage efficiency of zirconium-

- decorated biphenylene monolayer: A computational study, *Energy Storage* **4**, e377 (2022).
- ⁴⁶ L. Asadi, Z. Saadati, and M. Salehpour, Theoretical evaluation of Al-doped biphenylene nanosheet sensing properties toward gamma-butyrolactone, *Structural Chemistry* **33**, 1947 (2022).
- ⁴⁷ W.-S. Su and C.-H. Yeh, Theoretical investigation of methane oxidation reaction over a novel metal-free catalyst biphenylene network, *Diamond and Related Materials* **124**, 108897 (2022).
- ⁴⁸ H. K. Al-Jayyousi, M. Sajjad, K. Liao, and N. Singh, Two-dimensional biphenylene: a promising anchoring material for lithium-sulfur batteries, *Scientific Reports* **12**, 4653 (2022).
- ⁴⁹ T. Han, Y. Liu, X. Lv, and F. Li, Biphenylene monolayer: a novel nonbenzenoid carbon allotrope with potential application as an anode material for high-performance sodium-ion batteries, *Phys. Chem. Chem. Phys.* **24**, 10712 (2022).
- ⁵⁰ X.-W. Chen, Z.-Z. Lin, and X.-M. Li, Biphenylene network as sodium ion battery anode material, *Phys. Chem. Chem. Phys.* **25**, 4340 (2023).
- ⁵¹ K. Niu, Q. Fan, L. Chi, J. Rosen, J. M. Gottfried, and J. Björk, Unveiling the formation mechanism of the biphenylene network, *Nanoscale Horiz.* **8**, 368 (2023).
- ⁵² F. Lv, H. Liang, and Y. Duan, Funnel-shaped electronic structure and enhanced thermoelectric performance in ultralight $c_x(\text{BN})_{1-x}$ biphenylene networks, *Phys. Rev. B* **107**, 045422 (2023).
- ⁵³ N. Yang, H. Yang, and G. Jin, Interface-induced topological phase and doping-modulated bandgap of two-dimensional graphene-like networks, *Chinese Physics B* **32**, 017201 (2023).
- ⁵⁴ N. P. Armitage, E. J. Mele, and A. Vishwanath, Weyl and Dirac semimetals in three-dimensional solids, *Rev. Mod. Phys.* **90**, 015001 (2018).
- ⁵⁵ Y. Wang, E. Liu, H. Liu, Y. Pan, L. Zhang, J. Zeng, Y. Fu, M. Wang, K. Xu, Z. Huang, *et al.*, Gate-tunable negative longitudinal magnetoresistance in the predicted type-II Weyl semimetal WTe₂, *Nature communications* **7**, 13142 (2016).
- ⁵⁶ F. Chen, H. Lv, X. Luo, W. Lu, Q. Pei, G. Lin, Y. Han, X. Zhu, W. Song, and Y. Sun, Extremely large magnetoresistance in the type-II Weyl semimetal MoTe₂, *Physical Review B* **94**, 235154 (2016).
- ⁵⁷ N. Kumar, Y. Sun, N. Xu, K. Manna, M. Yao, V. Süß, I. Leermakers, O. Young, T. Förster, M. Schmidt, *et al.*, Extremely high magnetoresistance and conductivity in the type-II Weyl semimetals WP₂ and MoP₂, *Nature Communications* **8**, 1642 (2017).
- ⁵⁸ J. Lai, Y. Liu, J. Ma, X. Zhuo, Y. Peng, W. Lu, Z. Liu, J. Chen, and D. Sun, Broadband anisotropic photoresponse of the “hydrogen atom” version type-II Weyl semimetal candidate TaIrTe₄, *ACS nano* **12**, 4055 (2018).

- ⁵⁹ K. Sadhukhan, A. Politano, and A. Agarwal, Novel undamped gapless plasmon mode in a tilted type-II Dirac semimetal, *Physical Review Letters* **124**, 046803 (2020).
- ⁶⁰ D. L. Bergman, C. Wu, and L. Balents, Band touching from real-space topology in frustrated hopping models, *Physical Review B* **78**, 125104 (2008).
- ⁶¹ D. Leykam, A. Andreanov, and S. Flach, Artificial flat band systems: from lattice models to experiments, *Advances in Physics: X* **3**, 1473052 (2018).
- ⁶² J.-W. Rhim and B.-J. Yang, Classification of flat bands according to the band-crossing singularity of Bloch wave functions, *Physical Review B* **99**, 045107 (2019).
- ⁶³ J. Ma, J.-W. Rhim, L. Tang, S. Xia, H. Wang, X. Zheng, S. Xia, D. Song, Y. Hu, Y. Li, *et al.*, Direct observation of flatband loop states arising from nontrivial real-space topology, *Physical Review Letters* **124**, 183901 (2020).
- ⁶⁴ J.-W. Rhim and B.-J. Yang, Singular flat bands, *Advances in Physics: X* **6**, 1901606 (2021).
- ⁶⁵ Y. Hwang, J.-W. Rhim, and B.-J. Yang, Geometric characterization of anomalous Landau levels of isolated flat bands, *Nature communications* **12**, 6433 (2021).
- ⁶⁶ H. González-Herrero, J. M. Gómez-Rodríguez, P. Mallet, M. Moaied, J. J. Palacios, C. Salgado, M. M. Ugeda, J.-Y. Veuillen, F. Yndurain, and I. Brihuega, Atomic-scale control of graphene magnetism by using hydrogen atoms, *Science* **352**, 437 (2016).
- ⁶⁷ M. R. Slot, T. S. Gardenier, P. H. Jacobse, G. C. Van Miert, S. N. Kempkes, S. J. Zevenhuizen, C. M. Smith, D. Vanmaekelbergh, and I. Swart, Experimental realization and characterization of an electronic Lieb lattice, *Nature physics* **13**, 672 (2017).
- ⁶⁸ M. Møller, S. P. Jarvis, L. Guérinet, P. Sharp, R. Woolley, P. Rahe, and P. Moriarty, Automated extraction of single H atoms with STM: tip state dependency, *Nanotechnology* **28**, 075302 (2017).
- ⁶⁹ H. Touhara and F. Okino, Property control of carbon materials by fluorination, *Carbon* **38**, 241 (2000).
- ⁷⁰ S. K. Padamata, A. Yasinskiy, S. Stopic, and B. Friedrich, Fluorination of two-dimensional graphene: A review, *Journal of Fluorine Chemistry* **255-256**, 109964 (2022).
- ⁷¹ B. Wang, J. Wang, and J. Zhu, Fluorination of graphene: A spectroscopic and microscopic study, *ACS Nano* **8**, 1862 (2014).
- ⁷² X. Chen, K. Fan, Y. Liu, Y. Li, X. Liu, W. Feng, and X. Wang, Recent advances in fluorinated graphene from synthesis to applications: Critical review on functional chemistry and structure engineering, *Advanced Materials* **34**, 2101665 (2022).
- ⁷³ W. Feng, P. Long, Y. Feng, and Y. Li, Two-dimensional fluorinated graphene: Synthesis, structures,

properties and applications, *Advanced Science* **3**, 1500413 (2016).